

Parameterized Post-Friedmann Signatures of Acceleration in the CMB

Wayne Hu*

*Kavli Institute for Cosmological Physics, Department of Astronomy,
& Astrophysics, Enrico Fermi Institute, University of Chicago, Chicago IL 60637*

(Dated: October 25, 2018)

We extend the covariant, parametrized post-Friedmann (PPF) treatment of cosmic acceleration from modified gravity to an arbitrary admixture of matter, radiation, relativistic components and spatial curvature. This generalization facilitates the adaptation of Einstein-Boltzmann codes for solving CMB and matter perturbations in the linear regime. We use such a code to study the effect of metric evolution on the CMB through the integrated Sachs-Wolfe effect. We discuss the ability of modified gravity to alter the low multipole spectrum, including lowering the power in the quadrupole. From a principal component description of the primary metric ratio parameter, we obtain general constraints from WMAP on modified gravity models of the acceleration.

PACS numbers:

I. INTRODUCTION

In the absence of theoretically compelling models for the acceleration of the expansion, it is useful to have a parametrized description of possible deviations from the standard cosmological constant model. To explore modified gravity explanations of the acceleration we need a parametrized post-Friedmann (PPF) description of gravity that parallels the parametrized post-Newtonian description of solar system tests.

Many attempts to parametrize deviations phenomenologically (e.g. [1, 2, 3, 4, 5]) or across a limited range of scales (e.g. [6, 7, 8, 9, 10]) exist in the literature. Hu & Sawicki [11] recently introduced a PPF approach that spans all linear scales and includes an ansatz for non-linear phenomenology. The linear framework is based on enforcing the requirements of a metric theory, with small deviations from the Friedmann-Robertson-Walker metric, and covariant conservation of the stress energy tensor. This approach provides an excellent description of at least two specific models of modified gravity, the self-accelerating branch of the braneworld acceleration model (DGP [12]) and the modified action $f(R)$ model [13, 14, 15].

In this Paper, we extend the PPF approach to include relativistic matter components and spatial curvature. This generalization yields a self-consistent means of evolving metric perturbations from initial conditions in the radiation dominated era through to the present. We also phrase the PPF description in a manner that is useful for adapting an Einstein-Boltzmann code (e.g. [16, 17]) for modified gravity. Furthermore, specific modified gravity models already require such components at low redshift, e.g. the self-accelerating branch of DGP requires spatial curvature to fit distance measures [18] and the normal branch requires dark energy to explain acceleration.

We use this generalization to study the impact of evolution in the metric on the cosmic microwave background (CMB) through the integrated Sachs-Wolfe (ISW) effect. In the DGP and $f(R)$ models of cosmic acceleration it is well known that the ISW effect provides one of the most powerful and robust tests available [6, 18, 19, 20, 21, 22]. Since it arises from fluctuations near the horizon scale during the acceleration epoch, it requires a fully covariant description such as the one developed here. It also therefore tests gravity on the largest scales observable.

We begin in §II with the multicomponent generalization of the PPF description. This derivation is given in the comoving gauge but we describe in the Appendix the corresponding relations in the synchronous gauge. In §III we explore the phenomenology of the ISW effect in the CMB and examine current constraints. We discuss these results in §III D.

II. MULTICOMPONENT FORMALISM

In §II A, we adapt the structure of multicomponent covariant linear perturbation theory to modified gravity models. This treatment reduces to that of [11] in the limit of a flat, matter only universe. We discuss gauges relevant for the PPF parametrization in §II B and derive the explicit representation in §II C.

A. Covariant Structure

For the purposes of constructing a self-consistent covariant parametrization of modified gravity, it is convenient to view the modifications to gravity in terms of an additional “dark energy” stress tensor [6, 23]. Given a metric theory of gravity, we are always free to *define* the dark energy stress tensor to be

$$T_e^{\mu\nu} \equiv \frac{1}{8\pi G} G^{\mu\nu} - T_T^{\mu\nu}, \quad (1)$$

where we use the subscript “ T ” for the total stress energy tensor, which combines all true components, and “ e ” for

*Electronic address: w hu@background.uchicago.edu

the effective dark energy here and below. Note that we allow the total stress energy tensor to contain true dark energy components such as a cosmological constant or scalar fields for maximal generality (*cf.* [11]).

The effective dark energy behaves as a separately conserved system by virtue of the Bianchi identities and the conservation of $T_T^{\mu\nu}$ [24]

$$\nabla_\mu T_e^{\mu\nu} = \frac{1}{8\pi G} \nabla_\mu G^{\mu\nu} - \nabla_\mu T_T^{\mu\nu} = 0. \quad (2)$$

However the closure relation for this conservation law, which specifies the relationship between the components of the stress energy tensor, can and will in general depend on the matter content in contrast to minimally coupled dark energy models [11, 24, 25].

As usual, statistical isotropy requires that at the background level the stress tensors can be parametrized by the energy density and pressure

$$\begin{aligned} T_0^0 &= -\rho, \\ T_0^i &= 0, \\ T_j^i &= p\delta_j^i, \end{aligned} \quad (3)$$

for both the total and the effective stress energy tensor.

The background Einstein tensor is built out of the Friedmann-Robertson-Walker metric

$$ds^2 = g_{\mu\nu} dx^\mu dx^\nu = a^2(-d\eta^2 + \gamma_{ij} dx^i dx^j), \quad (4)$$

where $\eta = \int dt/a$ is the conformal time. In spherical coordinates γ_{ij} , the spatial metric with constant curvature K , can be represented as

$$\gamma_{ij} dx^i dx^j = dD^2 + D_A^2 d\Omega, \quad (5)$$

where $D_A = K^{-1/2} \sin(K^{1/2} D)$ is the angular diameter distance. The Einstein equation (1) becomes the usual Friedmann equation

$$H^2 + \frac{K}{a^2} = \frac{8\pi G}{3} (\rho_T + \rho_e). \quad (6)$$

The conservation laws

$$\begin{aligned} \rho'_T &= -3(\rho_T + p_T), \\ \rho'_e &= -3(\rho_e + p_e), \end{aligned} \quad (7)$$

close the system of equations for the background equations. The effective dark energy is thus parametrized in the same way as true dark energy: by the density today in units of critical $\Omega_e = 8\pi G \rho_e (\ln a = 0) / 3H_0^2$ and the effective equation of state $w_e(\ln a) = p_e / \rho_e$.

Scalar linear perturbations may be decomposed into the eigenfunctions of the Laplace operator

$$\nabla^2 Y = -k^2 Y, \quad (8)$$

and its covariant derivatives

$$\begin{aligned} Y_i &= (-k) \nabla_i Y, \\ Y_{ij} &= (k^{-2} \nabla_i \nabla_j + \gamma_{ij} / 3) Y. \end{aligned} \quad (9)$$

The most general scalar linear perturbations to the metric of a wavenumber k can be parametrized by [26, 27]

$$\begin{aligned} \delta g_{00} &= -a^2(2AY), \\ \delta g_{0i} &= -a^2 B Y_i, \\ \delta g_{ij} &= a^2(2H_L Y \gamma_{ij} + 2H_T Y_{ij}). \end{aligned} \quad (10)$$

Likewise the stress energy tensors can be parametrized as

$$\begin{aligned} \delta T_0^0 &= -\delta\rho, \\ \delta T_0^i &= -(\rho + p)vY^i, \\ \delta T_j^i &= \delta p Y \delta_j^i + p \Pi Y_j^i. \end{aligned} \quad (11)$$

We again describe the modification to gravity with an effective dark energy stress tensor and allow the total stress energy tensor to be composed of multiple components

$$\begin{aligned} \delta\rho_T &= \sum_i \delta\rho_i, \\ (\rho_T + p_T)v_T &= \sum_i (\rho_i + p_i)v_i, \\ \delta p_T &= \sum_i \delta p_i, \\ p_T \Pi_T &= \sum_i p_i \Pi_i. \end{aligned} \quad (12)$$

By definition, Eqn. (1) enforces the usual 4 Einstein field equations [28]

$$\begin{aligned} H_L + \frac{1}{3}H_T + \frac{B}{k_H} - \frac{H'_T}{k_H^2} &= \frac{4\pi G}{H^2 c_K k_H^2} \left[\delta\rho + 3(\rho + p) \frac{v - B}{k_H} \right], \\ A + H_L + \frac{H_T}{3} + \frac{B' + 2B}{k_H} - \left[\frac{H''_T}{k_H^2} + \left(3 + \frac{H'}{H} \right) \frac{H'_T}{k_H^2} \right] &= -\frac{8\pi G}{H^2 k_H^2} p \Pi, \\ A - H'_L - \frac{H'_T}{3} - \frac{K}{(aH)^2} \left(\frac{B}{k_H} - \frac{H'_T}{k_H^2} \right) &= \frac{4\pi G}{H^2} (\rho + p) \frac{v - B}{k_H}, \\ A' + \left(2 + 2\frac{H'}{H} - \frac{k_H^2}{3} \right) A - \frac{k_H}{3} (B' + B) &- H''_L - \left(2 + \frac{H'}{H} \right) H'_L = \frac{4\pi G}{H^2} (\delta p + \frac{1}{3} \delta\rho), \end{aligned} \quad (13)$$

where the stress energy components on the rhs combine the total and effective contributions. Here $' = d/d \ln a$, $k_H = (k/aH)$, and $c_K = 1 - 3K/k^2$. The conservation laws become the continuity and Navier-Stokes equations

$$\begin{aligned} \delta\rho'_i + 3(\delta\rho_i + \delta p_i) &= -(\rho_i + p_i)(k_H v_i + 3H'_L), \\ \frac{[a^4(\rho_i + p_i)(v_i - B)]'}{a^4 k_H} &= \delta p_i - \frac{2}{3} c_K p_i \Pi_i + (\rho_i + p_i) A, \end{aligned} \quad (14)$$

for all components separately conserved including the effective dark energy.

B. Gauge

The covariant Einstein and conservation equations (13) and (14) apply to any choice of gauge. For the PPF construction it is useful to work with variables that take on certain meanings such as curvature and potential fluctuations in specific gauges. For numerical codes it is useful to have a covariant representation of such variables so that they may be accessed from other gauge choices.

Under a gauge transformation defined by the change in conformal time slicing T and spatial threading L [26, 27]

$$\begin{aligned}\eta &= \tilde{\eta} + T, \\ x^i &= \tilde{x}^i + LY^i,\end{aligned}\quad (15)$$

the metric variables transform as

$$\begin{aligned}A &= \tilde{A} - aH(T' + T), \\ B &= \tilde{B} + aH(L' + k_H T), \\ H_L &= \tilde{H}_L - aH\left(T + \frac{1}{3}k_H L\right), \\ H_T &= \tilde{H}_T + aHk_H L,\end{aligned}\quad (16)$$

and the stress energy components transform as

$$\begin{aligned}\delta\rho &= \tilde{\delta\rho} - \rho' aHT, \\ \delta p &= \tilde{\delta p} - p' aHT, \\ v &= \tilde{v} + aHL', \\ \Pi &= \tilde{\Pi}.\end{aligned}\quad (17)$$

A gauge is fully specified if the functions T and L are uniquely defined.

Following [11], we shall construct the PPF description from a combination of (total matter or) comoving and Newtonian gauge quantities. The comoving gauge is specified by the conditions

$$\begin{aligned}B &= v_T, \\ H_T &= 0.\end{aligned}\quad (18)$$

They fully specify the gauge transformation from an alternate gauge choice

$$\begin{aligned}T &= (\tilde{v}_T - \tilde{B})/k, \\ L &= -\tilde{H}_T/k.\end{aligned}\quad (19)$$

To avoid confusion between fluctuations defined in different gauges, we will assign special variable names to comoving gauge quantities

$$\begin{aligned}\zeta &\equiv H_L, \\ \xi &\equiv A, \\ \rho\Delta &\equiv \delta\rho, \\ \Delta p &\equiv \delta p, \\ V &\equiv v.\end{aligned}\quad (20)$$

Δp should not be confused with $p\Delta = p(\delta\rho/\rho)$.

Similarly, the Newtonian gauge is defined by the condition $B = H_T = 0$ and the transformation

$$\begin{aligned}T &= -\frac{\tilde{B}}{k} + \frac{\tilde{H}'_T}{kk_H}, \\ L &= -\frac{\tilde{H}_T}{k}.\end{aligned}\quad (21)$$

To avoid confusion we define

$$\begin{aligned}\Phi &\equiv H_L, \\ \Psi &\equiv A.\end{aligned}\quad (22)$$

The relationships between the two metric fluctuations are

$$\zeta = \Phi - \frac{V_T}{k_H},\quad (23)$$

$$\xi = \Psi - \frac{V'_T + V_T}{k_H}.\quad (24)$$

We refrain from utilizing matter variables in Newtonian gauge but note that velocities in the two gauges are the same. We discuss the synchronous gauge representation in the Appendix.

C. PPF Parameterization

With the full covariant framework of linear perturbation theory in place, we now generalize the PPF description of the effective dark energy stress tensor [11] for multiple relativistic components and spatial curvature.

Following the original construction, we demand that the additional PPF contribution satisfy two requirements. On superhorizon scales $k_H \equiv k/aH \ll 1$, the curvature ζ in the comoving gauge is only altered by the effective dark energy at second order in k_H . Conservation of ζ in the absence of curvature and non-adiabatic stress fluctuations is a consequence of energy-momentum conservation [28] and applies to modified gravity models that satisfy it [29].

The third Einstein equation (13) reads

$$\zeta' = \xi - \frac{K}{(aH)^2} \frac{V_T}{k_H} - \frac{4\pi G}{H^2} (\rho_e + p_e) \frac{V_e - V_T}{k_H},\quad (25)$$

and the Navier-Stokes equation for the total velocity (14) gives

$$\xi = -\frac{\Delta p_T - \frac{2}{3}c_K p_T \Pi_T}{\rho_T + p_T}.\quad (26)$$

Without further loss of generality we can parametrize the effective dark energy contribution in this limit by a function $f_\zeta(a)$ where

$$\lim_{k_H \ll 1} \frac{4\pi G}{H^2} (\rho_e + p_e) \frac{V_e - V_T}{k_H} = -\frac{1}{3}c_K f_\zeta(a) k_H V_T\quad (27)$$

since $V_T = \mathcal{O}(k_H \zeta)$ for adiabatic fluctuations. The equation of motion for ζ in this limit now reads

$$\lim_{k_H \ll 1} \zeta' = -\frac{\Delta p_T - \frac{2}{3}c_K p_T \Pi_T}{\rho_T + p_T} - \frac{K}{k^2} k_H V_T + \frac{1}{3}c_K f_\zeta k_H V_T. \quad (28)$$

The second condition is that the metric satisfies a Poisson-like equation in the $k_H \gg 1$ quasistatic limit

$$\lim_{k_H \gg 1} \Phi_- = \frac{4\pi G}{c_K k_H^2 H^2} \frac{\Delta_T \rho_T + c_K p_T \Pi_T}{1 + f_G(a)}, \quad (29)$$

where f_G depends on time alone and $\Phi_- \equiv (\Phi - \Psi)/2$. To make these two limits compatible we introduce a parameter Γ such that

$$\Phi_- + \Gamma = \frac{4\pi G}{c_K k_H^2 H^2} [\Delta_T \rho_T + c_K p_T \Pi_T] \quad (30)$$

on all (linear) scales. Comparison with the first Einstein equation (13) for the Newtonian metric perturbations gives the first closure relation for the effective dark energy

$$\rho_e \Delta_e + 3(\rho_e + p_e) \frac{V_e - V_T}{k_H} + c_K p_e \Pi_e = -\frac{k^2 c_K}{4\pi G a^2} \Gamma. \quad (31)$$

Given that modified gravity models are most simply parametrized in terms of the relationship between Φ and Ψ that they induce, we describe the second closure condition through the effective anisotropic stress

$$\Phi_+ \equiv \frac{\Phi + \Psi}{2} = g(a, k) \Phi_- - \frac{4\pi G}{H^2 k_H^2} p_T \Pi_T. \quad (32)$$

Parametrizing this relation with a free function $g(a, k)$ again loses no further generality (*cf.* [6]). Without a modification to gravity $g = 0$. If the true anisotropic stress is negligible then $g = \Phi_+/\Phi_-$ and for this reason we will refer to it as the metric ratio parameter. Equation (32) defines the effective anisotropic stress as

$$\frac{4\pi G}{H^2 k_H^2} p_e \Pi_e = -g \Phi_-. \quad (33)$$

To complete these equations we must determine an equation of motion for Γ that is consistent with the two requirements (28) and (29). Taking the derivatives of Eqn. (23) and (30) with the help of the continuity and Navier-Stokes equations, we obtain the condition at $k_H \ll 1$

$$\lim_{k_H \ll 1} \Gamma' = S - \Gamma, \quad (34)$$

where the source

$$S = \frac{g' - 2g}{g + 1} \Phi_- + \frac{4\pi G}{(g + 1)k_H^2 H^2} \left\{ g[(p_T \pi_T)' + p_T \pi_T] - [(g + f_\zeta + g f_\zeta)(\rho_T + p_T) - (\rho_e + p_e)] k_H V_T \right\}. \quad (35)$$

Note that $S = 0$ if the modification to gravity vanishes: $g = 0$ and $f_\zeta = 0$.

In the opposite limit a comparison of Eqns. (29) and (30) imply

$$\lim_{k_H \gg 1} \Gamma = f_G \Phi_-. \quad (36)$$

To satisfy both limits, we take the equation of motion for Γ to be

$$(1 + c_\Gamma^2 k_H^2)[\Gamma' + \Gamma + c_\Gamma^2 k_H^2(\Gamma - f_G \Phi_-)] = S. \quad (37)$$

Substituting this relation into the derivative of the Poisson equation, we obtain

$$\zeta' = -\frac{\Delta p_T - \frac{2}{3}c_K p_T \Pi_T}{\rho_T + p_T} - \frac{K}{k^2} k_H V_T + \frac{g + 1}{F} \left[S - \Gamma' - \Gamma + f_\zeta \frac{4\pi G(\rho_T + p_T)}{H^2} \frac{V_T}{k_H} \right] \quad (38)$$

where

$$F(a) = 1 + 3(g + 1) \frac{4\pi G a^2}{k^2 c_K} (\rho_T + p_T). \quad (39)$$

Comparison with Eqn. (25) implicitly defines the effective dark energy momentum density

$$\frac{V_e - V_T}{k_H} = -\frac{H^2}{4\pi G(\rho_e + p_e)} \frac{g + 1}{F} \times \left[S - \Gamma' - \Gamma + f_\zeta \frac{4\pi G(\rho_T + p_T)}{H^2} \frac{V_T}{k_H} \right]. \quad (40)$$

Likewise the effective pressure can be defined from this relation through the dark energy Navier-Stokes equation

$$\frac{[a^4(\rho_e + p_e)(V_e - V_T)]'}{a^4 k_H} = \Delta p_e - \frac{2}{3}c_K p_e \Pi_e + (\rho_e + p_e)\xi. \quad (41)$$

This completes the multicomponent generalization of the PPF parametrization. It is described by three free functions $f_\zeta(\ln a)$, $f_G(\ln a)$ and $g(\ln a, k)$ and one parameter c_Γ in addition to the usual $w_e(a) = p_e(a)/\rho_e(a)$ which determines the background expansion. In the limit that the universe is spatially flat and relativistic matter components are subdominant, this description exactly matches the original treatment of [11].

In our numerical implementation, we evolve the density Δ_i and relative velocity $V_i - V_T$ components through the comoving gauge conservation equations and the Boltzmann hierarchy for the radiation closure condition and anisotropy using the code of [30, 31]. Specifically we evolve the comoving curvature fluctuation ζ through Eqn. (38) and ξ from the constraint Eqn. (26). The final metric perturbation is the total velocity $V_T (= B)$ which is evolved using the combined Newtonian and comoving Navier-Stokes equations [see also the gauge relation (23)]

$$V_T' + V_T = k_H(\Psi - \xi), \quad (42)$$

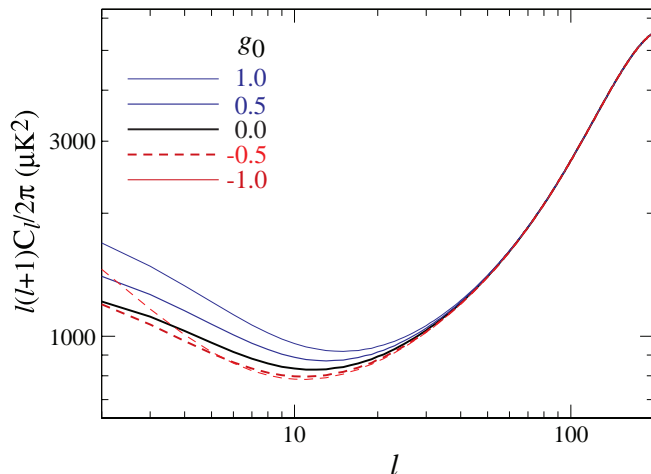


FIG. 1: CMB temperature power spectrum as a function of the amplitude of the metric ratio parameter today g_0 given the evolution described by Eqn. (44). Λ CDM corresponds to $g_0 = 0$. Increasing $|g_0|$ in the positive direction monotonically increases the ISW effect at low multipoles whereas in the negative direction it first decreases and then increases the effect. The other parameters have been fixed at $c_g = 0.01$, $c_T = 1$ and $w_e = -1$.

where Φ and Ψ are specified by Eqn. (30) and $g(\ln a, k)$. Finally Γ is obtained by evolving Eqn. (37). The second gauge relation of Eqn. (24) between ζ and Φ is used as a test of numerical accuracy.

Note that the relationship between Γ and $g(\ln a, k)$ and the effective energy density, anisotropic stress, momentum density and pressure fluctuations given by Eqns. (31), (33), (40) and (41) are only implicitly used. Likewise while the effective stress energy obeys the continuity and Navier-Stokes equations, they are not used in the numerical scheme. These relations are however useful for adapting the numerical scheme for the synchronous and other gauges (see Appendix).

III. PPF ISW EFFECT IN THE CMB

In general, our PPF description of cosmological deviations from general relativity includes one function of space and time that interrelate the metric fluctuations $g(\ln a, k)$, two functions of time only $f_G(\ln a)$ and $f_\zeta(\ln a)$ that determine the relationship between the metric and the matter, and one parametrized scale c_T that bridges the transition between the latter two relations. These free parameters allow a complex range of phenomena for the scale-dependent evolution of linear perturbations. The impact of such deviations on specific observables however limits the relevant parameters to a more manageable range.

Here we shall focus on the CMB temperature anisotropy induced by the evolution of the metric dur-

ing the acceleration epoch, the so-called the integrated Sachs-Wolfe (ISW) effect. This effect also highlights the extensions to the PPF description introduced in the previous sections. They allow an Einstein-Boltzmann code to self-consistently calculate the net CMB anisotropy from the initial epoch where radiation dominates through to the present.

Though the formalism allows for high redshift modifications of gravity, we work in the context that they only appear during the recent acceleration epoch. Hence the well-tested high multipole structure and polarization of the CMB are left unchanged.

In §III A we describe the impact of the PPF parameters on the low multipole temperature anisotropy of the ISW effect. We examine constraints on these parameters from WMAP in §III B and the reverse-engineering of models to produce specific features in the spectrum in §III C.

A. Phenomenology

We begin by specializing the PPF description for near horizon scale perturbations. The ISW effect is associated with the evolution of the metric potential Φ_- during the acceleration epoch of $z \lesssim 1$ and wavenumbers $k \sim 10^{-3} \text{ Mpc}^{-1}$. Correspondingly, it is important to characterize the PPF metric ratio parameter $g(\ln a, k)$ at such epochs and scales. Since $g(\ln a, k)$ should become independent of scale once $k_H \ll 1$ let us take the functional form

$$g(\ln a, k) = \frac{g_{\text{SH}}(\ln a)}{1 + (c_g k_H)^2}. \quad (43)$$

We shall use the parameter c_g to explore the range of scales that the ISW effect tests. We take $g \rightarrow 0$ for $k_H \gg 1$ and $f_G = 0$ so as to restore general relativity on small scales. Such models would evade all current constraints from large-scale structure and are uniquely probed by the CMB. On the other hand, we shall see that if $c_g \lesssim 0.01$ our constraints are valid for other choices since the high k behavior of g does not impact the ISW effect. In general, our treatment should be interpreted as constraining the average g during the acceleration epoch and for scales near the horizon regardless of its behavior on small scales.

Next, we assume that deviations in g will only appear when the modification to gravity becomes an important contributor to the expansion rate $H \propto \rho^{1/2}$. We therefore take a baseline functional form of

$$g_{\text{SH}}(\ln a) = g_0 \left(\frac{\rho_e \Omega_T}{\rho_T \Omega_e} \right)^{1/2} \quad (44)$$

such that $g_{\text{SH}}(0) = g_0$. In the self-accelerating branch of DGP, g grows to $g_0 \sim 1$ by the present on scales near the horizon and in the $f(R)$ models $g = -1/3$ on scales below a Compton wavelength that increases with time [11]. In the next section we will explore variations from the baseline functional form of Eqn. (44).

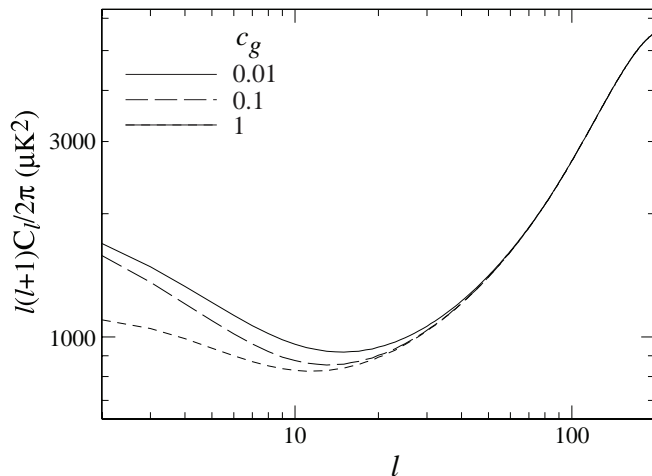


FIG. 2: Effect of changing the scale at which metric ratio deviations occur through c_g . Once $c_g \gtrsim 0.1$ deviations have been suppressed for $k \gtrsim 10^{-3} \text{Mpc}^{-1}$ where the ISW effect at the lowest multipoles peak. Other parameters have been fixed to $g_0 = 1$, $c_\Gamma = 1$ and $w_e = -1$.

The remaining important parameter is c_Γ which defines in units of the Hubble scale where the transition to the quasi-static Poisson equation occurs. We begin by choosing $c_\Gamma = 1$ as motivated by the DGP and $f(R)$ models [11].

Finally for definiteness we take $f_\zeta(\ln a) = 0.4g_{\text{SH}}(\ln a)$ for the relationship between the density Δ and metric fluctuations Φ_- on superhorizon scales (see [11] for a discussion). The ISW effect is insensitive to variations in this choice if $c_\Gamma \approx 1$.

We take $w_e = -1$ to illustrate effects that are coming purely from the modification of gravity and not the change in the expansion history. For the other cosmological parameters, we take the maximum likelihood values for WMAP3 [32]: $\Omega_m h^2 = 0.128$, $\Omega_b h^2 = 0.0223$, $\Omega_e = 0.76$, $\tau = 0.092$ with an initial power spectrum of

$$\frac{k^3 P_\zeta}{2\pi^2} = \delta_\zeta^2 \left(\frac{k}{0.05 \text{Mpc}^{-1}} \right)^{n-1} \quad (45)$$

with $\delta_\zeta = 4.56 \times 10^{-4}$ and $n = 0.958$.

We begin by exploring the impact of the amplitude of the metric deviation g_0 in Fig. 1 with the other parameters set to their fiducial values: $c_g = 0.01$, $c_\Gamma = 1$, $w_e = -1$. Note that $g_0 = 0$ is exactly equivalent to the Λ CDM model. For $g_0 > 0$ (solid lines), the ISW contributions increase monotonically since raising g_0 corresponds to increasing the decay of the potential Φ_- . For $g_0 < 0$, the decay is slowed and eventually turns into growth. Correspondingly, the ISW effect is first reduced and then enhanced as $|g_0|$ increases.

In Fig. 2, we illustrate the effect of suppressing g at high k through c_g in Eqn. (43) for $g_0 = 1$, $c_\Gamma = 1$ and $w_e = -1$. As c_g is raised beyond 0.1, the enhancement to

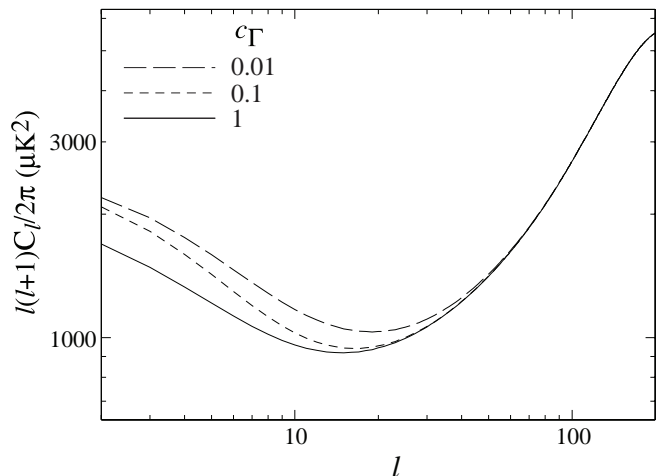


FIG. 3: Effect of changing the scale below which the quasistatic Poisson equation (29) holds through c_Γ . At a fixed metric ratio g , the ISW effect is enhanced by lowering c_Γ and delaying the onset of the quasistatic dynamics. The other parameters have been fixed to $g_0 = 1$, $c_g = 0.01$ and $w_e = -1$.

the ISW effect begins to go away. This confirms that the relevant scales at which g is constrained from the effect is near a tenth of the horizon scale or $k \sim 10^{-3} \text{Mpc}^{-1}$.

Changing the quasistatic transition scale through c_Γ has a substantial impact on the relationship between the metric ratio g and the ISW effect. As discussed in [11], the superhorizon impact of g implied by the conservation of the comoving curvature ζ tends to be substantially larger than the quasistatic limit would imply. In Fig. 3 we show the effect of decreasing c_Γ for $g_0 = 1$, $c_g = 0.01$ and $w_e = -1$. This extends the region where the superhorizon behavior hold. Once $c_\Gamma \lesssim 0.1$, wavenumbers relevant to the ISW effect are impacted leading to a substantial enhancement of the effect for the same g . The amount of enhancement then depends also on the superhorizon parameter f_ζ and we take $f_\zeta = 0.4g_{\text{SH}}$ throughout as an illustrative example. For the ISW effect f_ζ is largely degenerate with c_Γ since they both control the interpolation between the superhorizon behavior and quasistatic behavior both of which only depend on g [11].

Finally, in Fig. 4 we show the effect of varying the background expansion history for a fixed $g_0 = 1$, $c_g = 0.01$ and $c_\Gamma = 1$. Here Ω_e is adjusted to keep the distance to recombination fixed for the same $\Omega_m h^2$ and $\Omega_b h^2$ of the fiducial model. For the relatively small variations allowed by cosmological distance tests, the changes are small compared with cosmic variance and detectable variations in g .

B. Constraints

In the previous section, we have shown that for a given transition scale c_Γ , the ISW effect constrains the metric

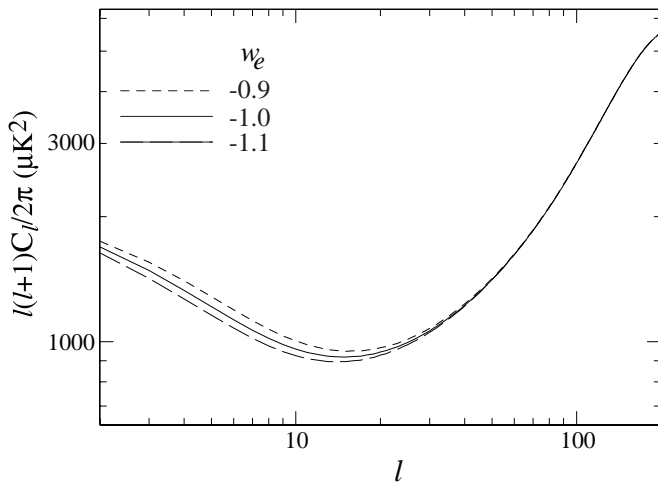


FIG. 4: Effect of changing the expansion history through w_e is small compared with cosmic variance and the effect of the PPF parameters for small deviations $-1.1 \leq w_e \leq -0.9$. The other parameters have been fixed to $g_0 = 1$, $c_g = 0.01$ and $c_\Gamma = 1$.

ratio parameter g at $k \sim 10^{-3} \text{ Mpc}^{-1}$ during the acceleration epoch. We can now assess how well WMAP constrains the amplitude of deviations in g . In lieu of a joint analysis of cosmological data sets that determine the distance redshift relation, we have here fixed the expansion history and other cosmological parameters to ΛCDM . Given how well most parameters are currently fixed, the most important caveat introduced by this assumption is that the initial power spectrum is taken to be of the power law form given by Eqn. (45). We shall return to this point below.

We begin by examining constraints on the amplitude parameter $g_0 = g(\ln a = 0)$ of Eqn. (44). The relative WMAP likelihood is shown in Fig. 5 for several choices of c_Γ and $c_g < 0.01$. Constraints tighten as c_Γ decreases due to the enhancement in the ISW effect shown in Fig. 3. A conservative interpretation of the constraint that is also well-motivated by the DGP and $f(R)$ examples would be to take $c_\Gamma = 1$. The distributions are all consistent with $g_0 = 0$. The statistically insignificant preference for negative g_0 is associated with a slight lowering of the low ℓ multipoles favored by the data as we discuss in the next section.

Even taking the conservative $c_\Gamma = 1$ limit, there is a problem in interpreting the constraint in a general context. The parameter g_0 represents the metric ratio today and is not directly constrained by the data. We have furthermore assumed an ad hoc evolution of g in Eqn. (44) motivated only by a rough scaling with the impact on the expansion rate.

In order to place more general constraints on the metric ratio g , we use a principal components construction to determine the temporal weights that the ISW effect actually constrain. The principal component construction

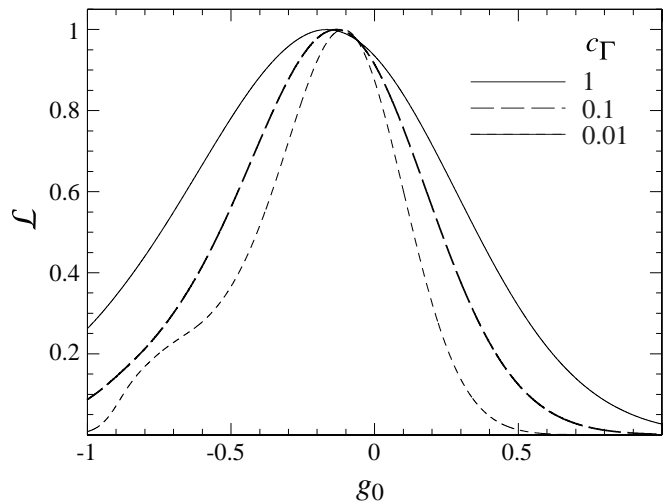


FIG. 5: WMAP likelihood of models as a function of g_0 for various c_Γ with $c_g = 0.01$ and other parameters fixed. Taking $c_\Gamma = 1$ provides conservative constraints. Normalization is arbitrary.

begins with the calculation of the Fisher matrix

$$F_{ij} = \sum_{\ell} (\ell + 1/2) \frac{\partial \ln C_{\ell}}{\partial p_i} \frac{\partial \ln C_{\ell}}{\partial p_j}, \quad (46)$$

where p_i are a set of N_p parameters that represent the values of a spline interpolated function $p(\ln a)$

$$g_{\text{SH}}(\ln a) = p(\ln a) \left(\frac{\rho_e}{\rho_T} \frac{\Omega_T}{\Omega_e} \right)^{1/2}, \quad (47)$$

evaluated at equally spaced intervals in $\ln a$. The derivatives are evaluated at the ΛCDM model of $p_i = 0$. We further take $c_g < 0.01$ and $c_\Gamma = 1$ here.

We then decompose the Fisher matrix into principal components indexed by μ

$$F_{ij} = \sum_{\mu} S_{i\mu} \sigma_{\mu}^{-2} S_{j\mu}, \quad (48)$$

where σ_{μ}^2 is the Fisher estimate of the variance of mode associated with the linear combination $\sum_i S_{i\mu} p_i$. Rank ordered in increasing variance, we find that the second mode has 5 times the variance of the first mode and so we shall use only the first mode in the following analysis.

More specifically, let us define a continuous function V_1 which is the high N_p limit of the discrete eigenmode

$$V_1(\ln a_i) \propto S_{i1}, \quad (49)$$

normalized so that

$$\int d \ln a V_1^2 = 1. \quad (50)$$

The metric ratio g that this mode represents is given by

$$g_1(\ln a) = \left(\frac{\rho_e}{\rho_T} \frac{\Omega_T}{\Omega_e} \right)^{1/2} V_1(\ln a) \quad (51)$$

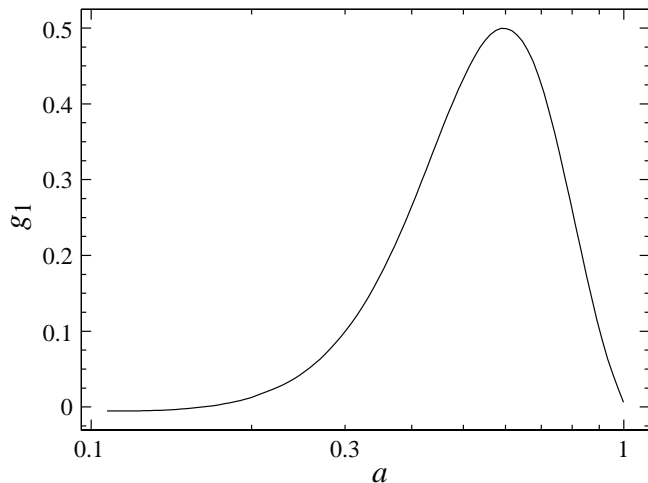


FIG. 6: First principal component g_1 of the metric ratio parameter as a function of scale factor a . Constraints derived from this component represent a temporal average of g of this functional form through Eqn. (54). Note that the maximum value $g_{\max} = 0.5$ at $z = 0.68$.

and is shown in Fig. 6. Note that the maximum value attained in this function is $g_{\max} = 0.5$ at a redshift of $z_{\max} = 0.68$. The ISW effect thus constrains a weighted average of g around z_{\max} . The falloff in sensitivity near the present epoch is due to projection effects.

We now use this functional form of g to evaluate the WMAP constraint on the amplitude g_{eff}

$$g_{\text{SH}}(\ln a) = g_{\text{eff}} \frac{g_1(\ln a)}{g_{\max}}. \quad (52)$$

Fig. 7 shows that the posterior probability distribution of g_{eff} is nearly Gaussian and that

$$g_{\text{eff}} = -0.12 \pm 0.27. \quad (53)$$

Note that g_{eff} is the value of g_{SH} at the z_{\max} .

Given a specific model for g , this constraint should be interpreted as one on a given weighted average of g around z_{\max} ; specifically

$$g_{\text{eff}} = g_{\max} \int d \ln a p(\ln a) V_1(\ln a). \quad (54)$$

For example, employing the model of Eqn. (44) we obtain $g_{\text{eff}} = 0.54g_0$. In Fig. 7 we show that the direct constraints on g_0 compare well with those inferred from g_{eff} .

C. Designer Models and Caveats

The constraints obtained in the previous section are fairly general in that a model that violates them while maintaining the underlying assumptions of a smooth initial power spectrum and an expansion history close to

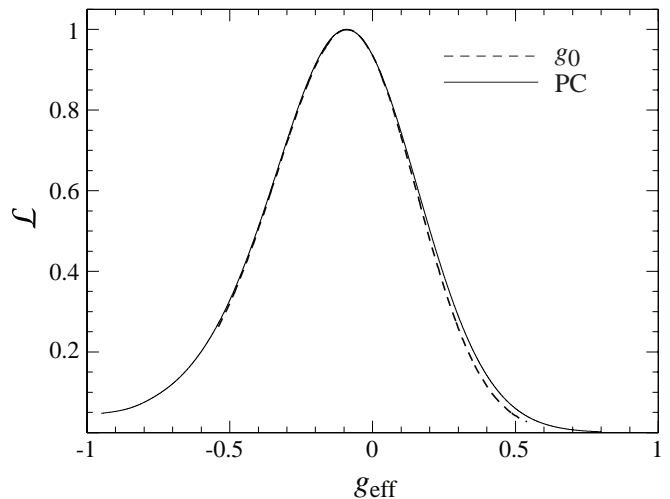


FIG. 7: WMAP constraints on g_{eff} from the first principal component. Note that g_{eff} is the maximum value of g attained by the principal component. For comparison the direct constraint on g_0 with $c_{\Gamma} = 0.1$ from Fig. 5 is overplotted with the conversion $g_{\text{eff}} = 0.54g_0$ from Eqn. (54).

Λ CDM will be disfavored by the data. However there remains a wide range of interesting phenomenology associated with acceptable models and a weakening of the underlying assumptions.

As an example of phenomenology that PPF models can produce that is not possible in Λ CDM, consider the statistical curiosity of the low quadrupole power in the CMB. Figure 8 shows that in the maximum likelihood Λ CDM model, the observed quadrupole is near the 95% cosmic variance limit. A quadrupole realization as extreme as the WMAP data only occurs in $\sim 5.5\%$ of the time. Of course in the first say 100 multipoles one expects and finds a few such events. The quadrupole is only special because it represents the largest observable scale and may hint at new physics beyond the standard cosmological model.

Construction of a model that sharply lowers the power in the quadrupole but not the octopole is hindered by the fact that in Λ CDM it gets nearly equal contributions from the ISW effect and the Sachs-Wolfe effect. These contributions are separated by a decade in physical scale making it difficult to invoke initial conditions as an explanation of the low quadrupole [33]. Furthermore for dynamical dark energy models based on scalar fields, it is difficult to reduce the ISW effect while maintaining an expansion history close to Λ CDM [34, 35].

As we have seen, a modified gravity model can alter the evolution of the metric even for an expansion history that is indistinguishable from Λ CDM. Let us then construct a model which nearly eliminates the ISW effect at low multipoles while leaving the spectrum at $\ell \gtrsim 10$ unchanged. To enhance the impact on the low multipoles let us take $c_{\Gamma} = 0.1$, $c_g < 0.01$ and take a very steep

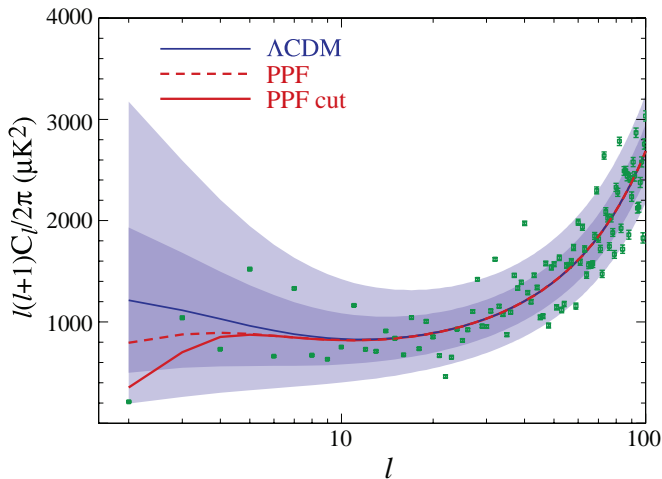


FIG. 8: Temperature power spectrum of the Λ CDM model with the WMAP data and noise error bars overplotted. Shaded regions represent the 68% and 95% cosmic variance intervals for the model. A PPF model constructed to eliminate the ISW effect can lower the power in the quadrupole. Shown is the model discussed in the text with and without an initial power spectrum cut off at $k_{\min} = 2.4 \times 10^{-4} \text{Mpc}^{-1}$.

evolution of g such that deviations appear only recently

$$g_{\text{SH}}(\ln a) = A \left(\frac{\rho_e}{\rho_T} \frac{\Omega_T}{\Omega_e} \right)^2. \quad (55)$$

We find that $A = -0.7$ causes a growth at late times that nearly offsets the earlier decay leaving the ISW effect nearly absent in the quadrupole. Because of the steep evolution, this model evades the constraints from the previous section. We show the spectrum of this model in Fig. 8 (dashed line). This model is a better fit to the WMAP data with a $\Delta 2 \ln L = -1.5$. Of course given the number of parameters and ad hoc assumptions of this model, such an improvement is not statistically significant. On the other hand, explorations of this sort can suggest what types of modified gravity models would be fruitful to study: in this case, models with $g < 0$ on the horizon scale near the present.

With the ISW effect nearly eliminated the quadrupole can be further lowered by a change in the initial power spectrum of Eqn. (45). Placing a cutoff of $k_{\min} = 2.4 \times 10^{-4} \text{Mpc}^{-1}$ produces the spectrum shown in Fig. 8 and an improved likelihood of $\Delta 2 \ln L = -2.8$.

This example also highlights the primary caveat of applying the constraint on g_{eff} in the previous section. That constraint assumes a featureless initial power spectrum where the constraints at high ℓ nearly fix the initial power at the horizon scale today. While this is reasonable given the expectation that gravity is only modified at late times, it remains an assumption nonetheless.

D. Discussion

We have generalized the parametrized post-Friedmann (PPF) description of cosmic acceleration from modified gravity to include multiple relativistic matter species and spatial curvature. This generalization facilitates the adaptation of Einstein-Boltzmann codes for modified gravity. We have adapted a comoving gauge code to study constraints on deviations from general relativity on the largest scales through the CMB.

The integrated Sachs-Wolfe (ISW) effect probes the evolution of the metric Φ_- on scales near the horizon during the acceleration epoch. Under the PPF parametrization, modifications to gravity can change the amplitude and shape of the ISW contributions to the low multipole CMB temperature power spectrum even if the expansion history is indistinguishable from that of a cosmological constant. For example in some regions of parameter space, the ISW effect can be nearly eliminated at the quadrupole bringing the predicted ensemble average quadrupole nearer to its observed value on our sky.

We use the WMAP data to constrain such modifications and find that deviations in the metric ratio parameter g are constrained at the level of $g_{\text{eff}} = -0.12 \pm 0.27$ at $z \sim 0.7$ and $k \sim 10^{-3} \text{Mpc}^{-1}$. Correspondingly, specific models such as the DGP and some $f(R)$ models are constrained by the data at levels consistent with the findings of previous work (e.g. [18, 20]). By phrasing these and other constraints in the model-independent PPF description, we gain a more general understanding of what aspects of general relativity are tested by the observations.

The modified gravity framework studied here should also enable future studies of other cosmological observables on large scales that are beyond the scope of this work such as the lensing of the CMB and faint galaxies as well as CMB-galaxy correlations.

APPENDIX A: SYNCHRONOUS GAUGE

Most public Boltzmann codes are written in the synchronous gauge (e.g. [16, 17]). For completeness, we outline here an implementation of PPF that is appropriate for such codes.

The synchronous gauge is defined by the conditions

$$\begin{aligned} A &= B = 0, \\ \eta_T &\equiv -\frac{1}{3}H_T - H_L, \\ h_L &= 6H_L, \\ T &= a^{-1} \int d\eta a \tilde{A} + c_1 a^{-1}, \\ L &= - \int d\eta (\tilde{B} + kT) + c_2. \end{aligned} \quad (\text{A1})$$

which leave two constants c_1 and c_2 to be specified by the initial choice of time slicing and threading (e.g. the

rest frame of the dark matter). On the other hand the gauge transformation from a specific synchronous gauge choice to the comoving gauge used in the main paper is completely defined

$$\begin{aligned} T &= (v_T^s/k), \\ L &= \frac{3}{k}(\eta_T + \frac{1}{6}h_L), \end{aligned} \quad (\text{A2})$$

where the superscript s denotes synchronous gauge quantities. Note further that the comoving gauge variables depend only on L' and not L since H_T vanishes in the comoving gauge.

The gauge transformation equations in the main text allow for the evolution of the dark energy parameter Γ to be expressed in terms of the synchronous gauge variables. We begin by expressing the comoving gauge density fluctuations as

$$\Delta_i \rho_i = \delta_i^s \rho_i - \rho_i' (v_T^s/k_H). \quad (\text{A3})$$

This allows us to obtain Φ_- in terms of δ_i^s , v_i^s and Γ . The sources for Γ must also be expressed in terms of synchronous gauge quantities. In addition to Φ_- and the gauge invariant π_i there is V_T . Starting with the gauge relation (23)

$$V_T = k_H(\Phi - \zeta), \quad (\text{A4})$$

we can then use the synchronous to comoving gauge relation

$$\zeta = -\eta_T - \frac{v_T^s}{k_H}, \quad (\text{A5})$$

and the metric relation implied by Eqn. (32)

$$\Phi = (g+1)\Phi_- - \frac{4\pi G}{H^2 k_H^2} p_T \Pi_T \quad (\text{A6})$$

to obtain

$$\frac{V_T}{k_H} = \frac{v_T^s}{k_H} + (g+1)\Phi_- - \frac{4\pi G}{H^2 k_H^2} p_T \Pi_T + \eta_T, \quad (\text{A7})$$

which now gives the evolution equation (37) for Γ in terms of synchronous variables only.

The conservation equations for the separate components of real matter and radiation are of course unaltered but require the evolution of h'_T and η_T from the Einstein equations. These are modified to include the stress energy of the effective dark energy. We can use the fluid correspondence and gauge relations to obtain

$$\delta_e^s = \Delta_e - 3(1+w_e) \frac{v_T^s}{k_H}. \quad (\text{A8})$$

Note that

$$v_e^s = V_e - V_T + v_T^s, \quad (\text{A9})$$

and is given by Eqn. (40) in terms of Φ_- , Γ , and V_T . Since $p_e \Pi_e$ is gauge invariant, the remaining component is the pressure fluctuation obtained from

$$\delta p_e^s = \Delta p_e + p_e' \frac{v_T^s}{k_H}. \quad (\text{A10})$$

The third and fourth Einstein equations (13) give

$$\begin{aligned} \eta_T' - \frac{3K}{k^2}(\eta_T' + \frac{1}{6}h_L') \\ = \frac{4\pi G}{H^2} \left[(\rho_T + p_T) \frac{v_T^s}{k_H} + (\rho_e + p_e) \frac{v_e^s}{k_H} \right], \end{aligned} \quad (\text{A11})$$

and

$$\begin{aligned} h_L'' + \left(2 + \frac{H'}{H} \right) h_L' \\ = -\frac{8\pi G}{H^2} [\delta_T^s \rho_T + 3\delta p_T^s + \delta_e^s \rho_T + 3\delta p_e^s]. \end{aligned} \quad (\text{A12})$$

Since the pressure perturbation δp_e^s is cumbersome to evaluate, one can alternately replace equation (A12) with the first Einstein equation (13)

$$h_L' = 2c_K k_H^2 \eta_T + \frac{8\pi G}{H^2} (\delta_T^s \rho_T^s + \delta_e^s \rho_e^s), \quad (\text{A13})$$

which involves v_e^s and $\delta_e \rho_e^s$ only. The latter system is the set of Einstein equations solved by CAMB [17].

The only drawback of using the latter system is that the matter density and metric h_L depend to leading order on the velocities of the effective (or real) dark energy through η_T even at $k_H \gg 1$ since the synchronous initial conditions typically set the dark matter velocity to zero. For example in ordinary smooth dark energy models, dark energy perturbations cannot be consistently set to zero in this set of equations when solving for the matter power spectrum whereas they may be in the former.

Acknowledgments: I thank Ignacy Sawicki and Yong-Seon Song for useful conversations and Wenjuan Fang for pointing out several typos in an earlier version. This work was supported by the U.S. Dept. of Energy contract DE-FG02-90ER-40560, the David and Lucile Packard Foundation and the KICP under NSF PHY-0114422.

[1] M. Ishak, A. Upadhye, and D. N. Spergel, Phys. Rev. **D74**, 043513 (2006), astro-ph/0507184.

[2] L. Knox, Y.-S. Song, and J. A. Tyson, Phys. Rev. **D74**,

- 023512 (2006).
- [3] S. Wang, L. Hui, M. May, and Z. Haiman (2007), arXiv:0705.0165 [astro-ph].
- [4] Y.-S. Song (2006), astro-ph/0602598.
- [5] D. Huterer and E. V. Linder, Phys. Rev. **D75**, 023519 (2007), astro-ph/0608681.
- [6] R. Caldwell, A. Cooray, and A. Melchiorri, Phys. Rev. **D76**, 023507 (2007), astro-ph/0703375.
- [7] L. Amendola, M. Kunz, and D. Sapone (2007), arXiv:0704.2421 [astro-ph].
- [8] P. Zhang, M. Liguori, R. Bean, and S. Dodelson, ArXiv e-prints **704** (2007), 0704.1932.
- [9] M. A. Amin, R. V. Wagoner, and R. D. Blandford (2007), arXiv:0708.1793 [astro-ph].
- [10] B. Jain and P. Zhang (2007), arXiv:0709.2375 [astro-ph].
- [11] W. Hu and I. Sawicki, Phys. Rev. **D76**, 104043 (2007), arXiv:0708.1190 [astro-ph].
- [12] G. R. Dvali, G. Gabadadze, and M. Porrati, Phys. Lett. **B485**, 208 (2000), hep-th/0005016.
- [13] S. M. Carroll, V. Duvvuri, M. Trodden, and M. S. Turner, Phys. Rev. **D70**, 043528 (2004), astro-ph/0306438.
- [14] S. Nojiri and S. D. Odintsov, Phys. Rev. **D68**, 123512 (2003), hep-th/0307288.
- [15] S. Capozziello, S. Carloni, and A. Troisi (2003), astro-ph/0303041.
- [16] U. Seljak and M. Zaldarriaga, Astrophys. J. **469**, 437 (1996), astro-ph/9603033.
- [17] A. Lewis, A. Challinor, and A. Lasenby, Astrophys. J. **538**, 473 (2000), astro-ph/9911177.
- [18] Y. Song, I. Sawicki, and W. Hu, Phys. Rev. D **75**, 064003 (2006), astro-ph/0606286.
- [19] A. Lue, R. Scoccimarro, and G. D. Starkman, Phys. Rev. **D69**, 124015 (2004), astro-ph/0401515.
- [20] Y. Song, H. Peiris, and W. Hu, Phys. Rev. D **76**, 063517 (2007), 0706.2399 [astro-ph].
- [21] F. Schmidt, M. Liguori, and S. Dodelson, Phys. Rev. **D76**, 083518 (2007), arXiv:0706.1775 [astro-ph].
- [22] L. Pogosian and A. Silvestri, Phys. Rev. **D77**, 023503 (2008), 0709.0296.
- [23] M. Kunz and D. Sapone, Phys. Rev. Lett. **98**, 121301 (2007), astro-ph/0612452.
- [24] S. Bashinsky (2007), arXiv:0707.0692 [astro-ph].
- [25] W. Hu, Astrophys. J. **506**, 485 (1998), astro-ph/9801234.
- [26] J. M. Bardeen, Phys. Rev. D **22**, 1882 (1980).
- [27] H. Kodama and M. Sasaki, Prog. Theor. Phys. Suppl. **78**, 1 (1984).
- [28] W. Hu and D. J. Eisenstein, Phys. Rev. D **59**, 083509 (1999), astro-ph/9809368.
- [29] E. Bertschinger, Astrophys. J. **648**, 797 (2006), astro-ph/0604485.
- [30] W. Hu and T. Okamoto, Phys. Rev. D **69**, 043004 (2003), astro-ph/0308049.
- [31] W. Hu, U. Seljak, M. White, and M. Zaldarriaga, Phys. Rev. D **57**, 3290 (1998), astro-ph/9709066.
- [32] D. N. Spergel et al. (WMAP), Astrophys. J. Suppl. **170**, 377 (2007), astro-ph/0603449.
- [33] C. Contaldi, M. Peloso, L. Kofman, and A. Linde, JCAP **0307**, 002 (2003), astro-ph/0303636.
- [34] C. Gordon and W. Hu, Phys. Rev. D **70**, 083003 (2004), astro-ph/0406496.
- [35] R. Bean and O. Dore, Phys. Rev. D **69**, 083503 (2004), astro-ph/0307100.